

# Three-dimensional flexible and conductive interconnected graphene networks grown by chemical vapour deposition

Zongping Chen<sup>†</sup>, Wencai Ren<sup>†</sup>, Libo Gao, Bilu Liu, Songfeng Pei and Hui-Ming Cheng<sup>★</sup>

**Integration of individual two-dimensional graphene sheets<sup>1–3</sup> into macroscopic structures is essential for the application of graphene. A series of graphene-based composites<sup>4–6</sup> and macroscopic structures<sup>7–11</sup> have been recently fabricated using chemically derived graphene sheets. However, these composites and structures suffer from poor electrical conductivity because of the low quality and/or high inter-sheet junction contact resistance of the chemically derived graphene sheets. Here we report the direct synthesis of three-dimensional foam-like graphene macrostructures, which we call graphene foams (GFs), by template-directed chemical vapour deposition. A GF consists of an interconnected flexible network of graphene as the fast transport channel of charge carriers for high electrical conductivity. Even with a GF loading as low as ~0.5 wt%, GF/poly(dimethyl siloxane) composites show a very high electrical conductivity of ~10 S cm<sup>-1</sup>, which is ~6 orders of magnitude higher than chemically derived graphene-based composites<sup>4</sup>. Using this unique network structure and the outstanding electrical and mechanical properties of GFs, as an example, we demonstrate the great potential of GF/poly(dimethyl siloxane) composites for flexible, foldable and stretchable conductors<sup>12</sup>.**

Graphene is a two-dimensional monolayer of carbon atoms packed into a honeycomb lattice that possesses a wealth of new physics<sup>1–3,13,14</sup> and many fascinating properties such as giant electron mobility<sup>2,13,14</sup>, extremely high thermal conductivity<sup>15</sup> and extraordinary elasticity and stiffness<sup>16</sup>. To harness these properties for macroscopic applications, both large-scale synthesis and integration of individual graphene sheets to advanced multifunctional structures are required. Since the report of isolated graphene prepared by simple mechanical cleavage of graphite crystals<sup>2</sup>, many approaches have been developed for the synthesis of graphene, including epitaxial growth on SiC or metals<sup>17,18</sup>, chemical exfoliation of graphite oxide<sup>4,7,19</sup>, liquid-phase ultrasonic exfoliation of graphite powder<sup>20</sup> and chemical vapour deposition (CVD) growth on metal substrates<sup>21–25</sup>. Owing to the ease of preparation and processing, chemically derived graphene sheets have been extensively used for integration with other materials such as polymers and self-assembly into various macroscopic structures, such as paper-like materials<sup>7</sup> with superior stiffness and strength, flexible transparent and conductive films<sup>8,9</sup> and three-dimensional (3D) macroporous structures<sup>10,11</sup> to extend their functions and achieve specific applications. However, these integrated graphene materials and structures show poor electrical conductivity owing to severe structural defects in

graphene sheets introduced during exfoliation and reduction processes and/or high inter-sheet junction contact resistance. Recently, large-area high-quality graphene films have been grown by CVD and transferred for macroscopic use as transparent conductive films<sup>24,26</sup>, which are far superior to those fabricated using chemically derived graphene sheets. However, both large-quantity synthesis of CVD-grown graphene and integration into 3D structures still remain a great challenge.

In this work, we develop a general strategy for the synthesis of a 3D graphene macroscopic structure with a foam-like network—graphene foam (GF), using template-directed CVD. Different from structures formed with small pieces of chemically derived graphene sheets, the GF fabricated by our approach is a monolith of a graphene 3D network, in which charge carriers can move rapidly with a small resistance through the high-quality and continuous CVD-grown graphene building blocks. Therefore, we expect to observe extraordinary electrical and mechanical properties of GFs and GF-based composites.

The synthesis of GF and its integration with polymers are illustrated in Fig. 1 and Supplementary Fig. S1. We chose nickel foam, a porous structure with an interconnected 3D scaffold of nickel (Fig. 1a), as a template for the growth of GFs. In brief, carbon was introduced into a nickel foam by decomposing CH<sub>4</sub> at 1,000 °C under ambient pressure, and graphene films were then precipitated on the surface of the nickel foam<sup>21,23,24</sup> (Fig. 1b and Supplementary Fig. S2). Because of the difference between the thermal expansion coefficients of nickel and graphene, ripples and wrinkles were formed on the graphene films<sup>22</sup> (Supplementary Fig. S2). Similar to the wrinkles in chemically derived graphene sheets<sup>5</sup>, these ripples and wrinkles probably result in an improved mechanical interlocking with polymer chains, and consequently better adhesion, when a GF is integrated with a polymer to form composite materials.

To obtain GFs, before etching away the nickel skeleton by a hot HCl (or FeCl<sub>3</sub>) solution, a thin layer of poly(methyl methacrylate) (PMMA) was deposited on the surface of the graphene films as a support to prevent the graphene network from collapsing during nickel etching (Fig. 1c,d). After the PMMA layer was carefully removed by hot acetone, a GF, a monolith of a continuous and interconnected graphene 3D network, was obtained (Figs. 1e, 2 and Supplementary Fig. S3), although a small shrinkage of the graphene skeleton occurs. The GF copies inherit the interconnected 3D scaffold structure of the nickel foam template, and all the graphene sheets in the GF are in direct contact with one another without breaks and are well separated. The use of the PMMA support layer

Shenyang National Laboratory for Materials Science, Institute of Metal Research, Chinese Academy of Sciences, Shenyang 110016, China. <sup>†</sup>These authors contributed equally to this work. \*e-mail: cheng@imr.ac.cn.

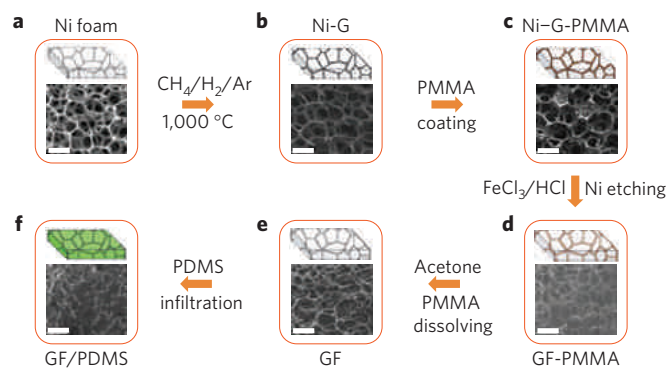


**Figure 1 | Synthesis of a GF and integration with PDMS.** **a, b,** CVD growth of graphene films (Ni-G, **b**) using a nickel foam (Ni foam, **a**) as a 3D scaffold template. **c,** An as-grown graphene film after coating a thin PMMA supporting layer (Ni-G-PMMA). **d,** A GF coated with PMMA (GF-PMMA) after etching the nickel foam with hot HCl (or  $\text{FeCl}_3/\text{HCl}$ ) solution. **e,** A free-standing GF after dissolving the PMMA layer with acetone. **f,** A GF/PDMS composite after infiltration of PDMS into a GF. All the scale bars are 500  $\mu\text{m}$ .

is critical to prepare a free-standing GF; only a severely distorted and deformed GF was obtained without the PMMA support layer (Supplementary Fig. S4). Moreover, the GF becomes thinner than the original nickel foam ( $\sim 1.2$  mm in thickness) after removing it from the acetone owing to the liquid capillary force caused by acetone evaporation<sup>27</sup>. With increasing number of graphene layers, the thickness of the GF is increased from  $\sim 100$  to  $\sim 600$   $\mu\text{m}$  (Supplementary Fig. S5), because of the lower shrinkage of the GF owing to the increased stiffness of thicker graphene sheets. This results in a higher porosity of GF, and consequently a lower volume or weight fraction of GF in GF/poly(dimethyl siloxane) (PDMS) composites (Fig. 3).

The free-standing GF is extremely light and flexible. For example, the GF obtained with a  $\text{CH}_4$  concentration of 0.7 vol% has an ultralow density of  $\sim 5$   $\text{mg cm}^{-3}$  (Supplementary Fig. S5), close to that of the lightest aerogel ( $2\text{--}3$   $\text{mg cm}^{-3}$ ), and corresponding to a high porosity of  $\sim 99.7\%$ . The GF also has a very high specific surface area, up to  $\sim 850$   $\text{m}^2 \text{g}^{-1}$ , corresponding to an average number of layers of  $\sim 3$  (Supplementary Fig. S5). Low-magnification transmission electron microscopy (TEM) observations indicate that the ripples and wrinkles in the graphene building blocks of the GF are preserved after removing the nickel skeleton (Fig. 2c). High-resolution TEM images show that the GF consists of mono- to few-layer graphene sheets (Fig. 2d), which is consistent with Raman measurements<sup>23,24,28</sup> (Fig. 2e) and that deduced from the specific surface area shown above (Supplementary Information). The non-uniformity is attributed to the polycrystalline nature of the nickel foam, in which individual nickel grains may independently affect the thickness of the graphene film during CVD (ref. 23). In addition, the Raman spectra measured on free-standing GFs show a strongly suppressed defect-related D band, indicating overall high quality of the graphene in GFs.

Our preparation process shows great versatility in controlling both the macrostructure and the microstructure of GFs. For example, we can tune the networks and pore structures of GFs by using different nickel foams (Supplementary Fig. S6). The average number of graphene layers, specific surface area and density of GFs can be controlled by changing  $\text{CH}_4$  concentration. Higher  $\text{CH}_4$  concentration leads to an increase in the number of graphene layers (Supplementary Fig. S7), and consequently a great change in the specific surface area, density and electrical conductivity of GFs (Supplementary Fig. S5 and Fig. 3c). Using Cu foams as template, we prepared GFs with monolayer graphene sheets

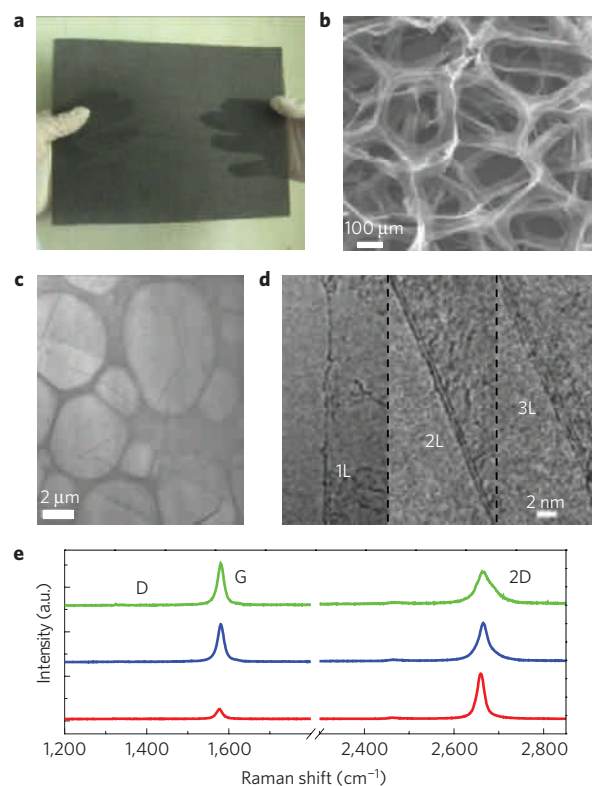


**Figure 2 | Characterization of a free-standing GF.** **a,** Photograph of a  $170 \times 220$   $\text{mm}^2$  free-standing GF. **b,** SEM image of a GF. **c,** Low-magnification TEM image of a GF. **d,** High-resolution TEM images of graphene sheets with different numbers of layers in a GF; the interlayer spacing of bilayer (2L) and trilayer (3L) graphene is  $\sim 0.34$  nm. **e,** Typical Raman spectra of a GF. The bottom spectrum and the other two correspond to monolayer and few-layer graphene, respectively, which are estimated from the intensity, shape and position of the G band and 2D band. The GF was prepared with a  $\text{CH}_4$  concentration of 0.7 vol%.

owing to the surface-catalysed growth mechanism of graphene on Cu (ref. 25). However, such a GF tends to collapse and break because its building blocks, monolayer graphene, are not able to bear the liquid capillary force caused by acetone evaporation (Supplementary Fig. S8). In addition, the size and quantity of GFs can be easily scaled up by using large nickel foam substrates, large reaction systems and a substrate-rolling synthesis strategy<sup>26</sup>. For example, we prepared a large GF with an area of  $170 \times 220$   $\text{mm}^2$  by using a large CVD furnace equipped with a quartz tube 71 mm in inner diameter (Fig. 2a).

Constructing an infinite connected network of conducting fillers in an insulating matrix is important to improve the electrical conductivity of composites. The unique interconnected network of GFs provides a great potential for use in composite materials for electrical applications. As an example, we fabricated GF/PDMS composites by infiltrating GFs with PDMS (Figs 1f and 3a). The composites show good flexibility, and can be bent, stretched and twisted without breaking (Supplementary Fig. S9). The scanning electron microscopy (SEM) images of the fracture surface of the composites show that the GFs adhere well to the PDMS matrix (Fig. 3b). Introduction of the PDMS matrix does not damage the interconnected 3D scaffold of GFs, as demonstrated in Fig. 3c, because the electrical conductivity of GFs shows nearly no change after infiltration with PDMS. In chemically derived graphene-based polymer composites, small pieces of graphene sheets are randomly distributed inside the polymer matrix and surrounded by the molecular chains of the polymer. As a result,

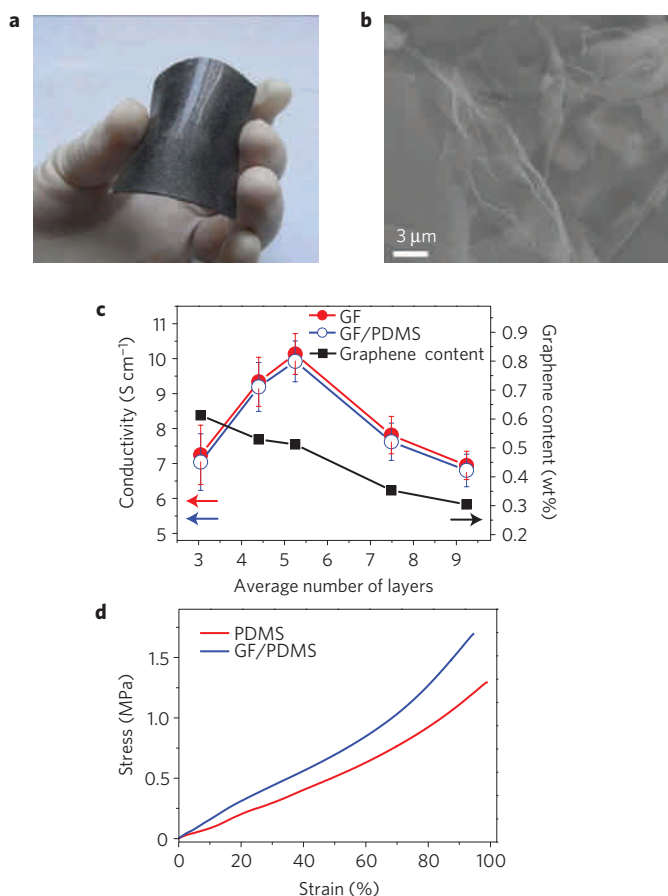


**Figure 3 | Morphology, fracture surface, electrical conductivity and mechanical properties of GF/PDMS composites.** **a**, Photograph of a bent GF/PDMS composite, showing its good flexibility. **b**, SEM image of the fracture surface of the composite. **c**, Electrical conductivity of GFs and GF/PDMS composites as a function of the number of graphene layers (Corresponding to different weight fractions of GFs in the composites). The average conductivity of GFs and GF/PDMS composites was calculated over five specimens for each sample and error bars for standard deviation are shown. **d**, Typical stress-strain curves of PDMS and GF/PDMS composites with  $\sim 0.5$  wt% graphene loading.

the electrical conductivity of these composites strongly relies on electron percolation between the separated graphene sheets. Combined with the relatively low quality of chemically derived graphene sheets, these composite materials have low electrical conductivity<sup>4,6</sup>. In contrast, because electrons can move very quickly through the seamlessly interconnected 3D GF network of high-quality graphene, our GF/PDMS composites show a very high electrical conductivity of  $\sim 10 \text{ S cm}^{-1}$  at an ultralow graphene loading of  $\sim 0.5$  wt% ( $\sim 0.22$  vol%). This value is  $\sim 6$  orders of magnitude higher than that of chemically derived graphene-based composites<sup>4</sup> and also much higher than those of carbon nanotube (CNT) composites at the same loading fraction (Supplementary Table S1), showing great advantages of GFs in the use of composites for electrical applications.

Because of the competition between the resistance decrease and thickness increase of the GF with increasing number of graphene layers (Supplementary Fig. S10), the electrical conductivity of GF and GF/PDMS composites does not show a monotonic increase with the number of graphene layers and graphene fraction in the composite (Fig. 3c). The resistance decrease of the GF with number of layers tends to level out after about five layers, whereas the thickness of the GF continues to grow at the same pace even above

five layers. Therefore, the GF and GF/PDMS composites show an optimal average number of graphene layers of about five for the maximum conductivity as shown in Fig. 3c. Incorporating other kinds of polymer such as epoxy resin with GFs was also carried out, and the composites obtained have an electrical conductivity similar to that of GF/PDMS at the same graphene loading. Furthermore, the GF also obviously improves the mechanical properties of the PDMS matrix (Fig. 3d and Supplementary Fig. S11). The ultimate strength of the GF/PDMS composites is increased by a factor of  $\sim 1.3$  compared with the pure PDMS.

The simultaneous incorporation of excellent mechanical robustness and electronic performance is the key to realizing stretchable electronics<sup>29</sup>. A GF has the following characteristics: high electrical conductivity, good mechanical robustness, potential flexibility and stretchability. Therefore, a GF is perfect for high-performance stretchable conductors. However, conventional conductors such as metallic foils and thin films have poor mechanical robustness and elasticity despite higher electrical conductivity<sup>29</sup>, which make them not suitable for stretchable conductors. For example, the nickel foams we used show a high electrical conductivity of  $\sim 350 \text{ S cm}^{-1}$ , but the nickel foam/PDMS composites could not recover to their initial form after even slight bending or stretching, and start to break at  $\sim 50\%$  stretching (Supplementary Figs S12 and S13). Constructing specific structural layouts and developing new electronic materials are two conceptually different, but complementary, ways to achieve stretchable electronics<sup>12</sup>. The excellent electrical and mechanical properties of the GF/PDMS composites and the unique network structure of GFs combines the advantages of both material and structural layout, which gives GF/PDMS composites great potential for use as flexible and stretchable conductors (Fig. 4), a key component of stretchable and curvilinear large-area electronics such as sensory skins for robotics, structural health monitors and wearable communication devices<sup>12</sup>.

We investigated the effect of bending and stretching on the electrical resistance of the composite with a  $\sim 0.5$  wt% GF loading, which has the best electrical conductivity among all the GF/PDMS composites prepared. The bend and stretch tests were carried out with a home-made two-point bending device and a high-precision mechanical system. The electrical resistance shows a small increase up to a bend radius of 2.5 mm and can perfectly recover after straightening (Fig. 4a). Notably, after 10,000 cycles for a bend radius of 2.5 mm, the resistance only increases  $\sim 2.7\%$  (Fig. 4a inset). Even for a very small bend radius of  $\sim 0.8$  mm, although the resistance of the composite is increased through the first three cycles of bending and straightening, it becomes stable (Fig. 4b) and the electrical resistance increase remains constant at only  $\sim 7\%$  from the fourth cycle under bending, compared with that when straightening (Fig. 4b inset). These results show the excellent electromechanical stability of GF/PDMS composites compared with conventional materials used in flexible electronics, even graphene films<sup>24</sup>.

We further investigated the electrical and mechanical properties of GF/PDMS composites by measuring their electrical resistance as a function of uniaxial tensile strain. Figure 4c shows the results at a maximum strain of 50%. Similar to the results in the bending experiments, the resistance of the composites increases with stretching but their resistance change becomes stable after the fifth cycle of stretch-release. From the sixth cycle, the electrical resistance is restored to a constant value when the strain is released, with a resistance increase of  $\sim 30\%$  under 50% stretching (Fig. 4c inset). The irreversible resistance increase is larger for a larger maximum tensile strain (Supplementary Fig. S14), indicating that it can be intrinsically attributed to the partial breaking or cracking of the GF network. Moreover, the number of cycles needed for GF/PDMS conductors to become stable also depends on the degree of mechanical deformation (Supplementary Fig. S14). Under larger maximum deformation, more cycles are needed for the GF/PDMS conductors

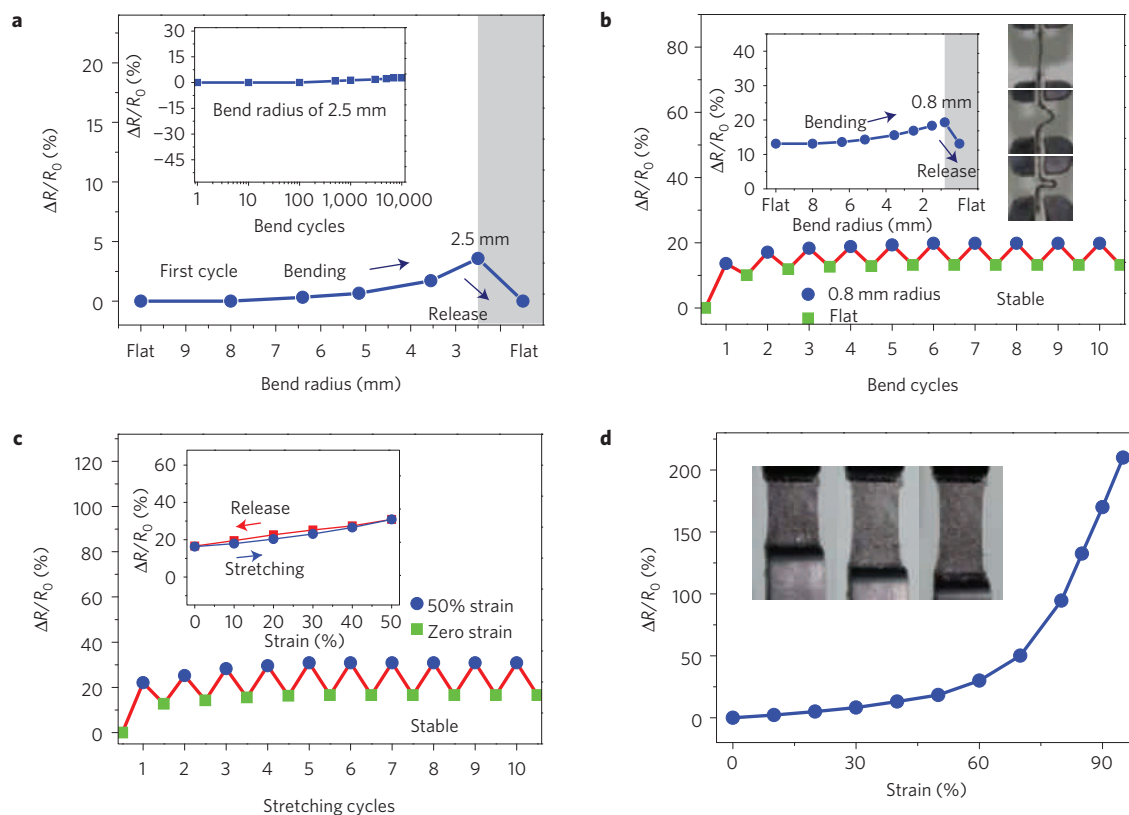


**Figure 4 | Electrical-resistance change of GF/PDMS composites under mechanical deformation.** **a**, Electrical-resistance variation of a composite at a bend radius up to 2.5 mm in the first bend cycle. The inset shows the resistance change of the composite as a function of bend cycles for a bend radius of 2.5 mm. **b**, Electrical-resistance change of a composite when bending to a radius of 0.8 mm and then straightening for each cycle. The resistance change becomes stable after the third cycle. The left inset shows the resistance variation of the composite in a typical bend cycle after becoming stable. The right inset shows the bending process. **c**, Electrical-resistance change of a composite after 50% stretching and then releasing for each cycle. In each cycle, the composite was gradually stretched to a strain of 50% and then released to zero strain with the same stretching rate of  $0.5 \text{ mm min}^{-1}$ . The resistance change becomes stable after the fifth cycle. The inset shows the resistance variation of the composite in a typical stretch/release cycle after becoming stable. **d**, Electrical-resistance variation of the composite as a function of uniaxial tensile strain until fracture. The inset shows the stretching process. Multiple GF/PDMS composites were measured, and the electrical-resistance change shows a good reproducibility under the same mechanical deformation. The loading of GF in the PDMS matrix is  $\sim 0.5 \text{ wt\%}$  for all the measured composites.  $R_0$  refers to the electrical resistance of the pristine composite, and  $\Delta R$  refers to the resistance change of the bent or stretched composite relative to that of the pristine composite.

to become stable. Further stretching of the sample results in a steep increase of the resistance until the sample breaks at  $\sim 95\%$  strain (Fig. 4d). These results show that the electromechanical properties of the GF/PDMS composites under stretching are far superior to those of graphene films grown by CVD, which show mechanical failure over 6% strain on an unstrained PDMS substrate and an order-of-magnitude increase in resistance at  $\sim 25\%$  strain on a pre-stretched PDMS substrate<sup>24</sup>. These results are comparable to those of both elastic conductors fabricated using aligned CNT arrays<sup>30</sup> and CNT-based composites with a high loading ( $\sim 20 \text{ wt\%}$ ) of CNTs (ref. 29), and indicate the great potential of GF/PDMS composites for high-performance elastic conductors.

In summary, we have developed a template-directed CVD technique for the fabrication of macroscopic 3D GF structures using nickel foams as templates. The graphene sheets in the GFs are seamlessly interconnected into a 3D flexible network. The high quality of the graphene sheets and their perfect connection in three dimensions give the material outstanding electrical conductivity that is superior to that of macroscopic graphene structures from chemically derived graphene sheets. The unique network structure, high specific surface area and outstanding electrical and mechanical properties of GFs and their composites should enable many applications including high-performance electrically conductive polymer composites, elastic and flexible conductors,

electrode materials for lithium ion batteries and supercapacitors, thermal management, catalyst and biomedical supports and so on. Moreover, this template-directed CVD technique is versatile and scalable, and can be a general strategy for fabricating a broad class of 3D macroscopic graphene structures of determined shapes with excellent properties and new uses.

## Methods

**Fabrication of GFs and GF/PDMS composites.** Nickel foams (Alantum Advanced Technology Materials (Shenyang),  $\sim 320 \text{ g l}^{-2}$  in areal density and  $\sim 1.2 \text{ mm}$  in thickness) were used as 3D scaffold templates for the CVD growth of GF. They were cut into pieces of  $20 \times 20 \text{ mm}^2$  and placed in a quartz tube of outer diameter 25 mm and inner diameter 22 mm. The nickel foams were heated to  $1,000^\circ \text{C}$  in a horizontal tube furnace (Lindberg Blue M, TF55030C) under Ar (500 s.c.c.m.) and  $\text{H}_2$  (200 s.c.c.m.) and annealed for 5 min to clean their surfaces and eliminate a thin surface oxide layer. A small amount of  $\text{CH}_4$  was then introduced into the reaction tube at ambient pressure. The flow rates of  $\text{CH}_4$  used were 2, 3.5, 5, 7 and 10 s.c.c.m., corresponding to concentrations of 0.3, 0.5, 0.7, 1.0 and 1.4 vol% in the total gas flow, respectively. After 5 min of reaction-gas mixture flow, the samples were rapidly cooled to room temperature at a rate of  $\sim 100^\circ \text{C min}^{-1}$  under Ar (500 s.c.c.m.) and  $\text{H}_2$  (200 s.c.c.m.). The size and quantity of GFs can be easily scaled up by using large nickel foam substrates and large reaction systems. For example, we prepared a large GF with a size of  $170 \times 220 \text{ mm}^2$  (Fig. 2a) by using a large piece of nickel foam with the same size, which was rolled up and inserted into a large CVD furnace (Lindberg Blue M, HTF55347C) equipped with a quartz tube 71 mm in inner diameter. The CVD growth conditions are the same as those used in the small furnace, except for doubling the flow rate of

each gas. To prevent structural failure of the GF when the nickel was etched away, a thin PMMA layer was used as a support to reinforce the graphene structure. The Ni foams covered with graphene were drop-coated with a PMMA solution (weight-averaged molecular mass  $M_w = 996,000$ , 4 wt% in ethyl lactate), and then baked at 180 °C for 30 min. This process solidified the PMMA to form a thin film on the graphene surface (Ni-G-PMMA). Then the samples were put into a HCl (3 M) (or  $\text{FeCl}_3/\text{HCl}$ , 1 M/1 M) solution at 80 °C for 3 h to completely dissolve the nickel to obtain GF-PMMA. Finally free-standing GFs were obtained by dissolving the PMMA with hot acetone at 55 °C.

GF/PDMS composites were fabricated by infiltrating the free-standing GFs with PDMS prepolymer, a viscous mixture of base/curing agent (Sylgard 184, Dow Corning), followed by degassing in a vacuum oven for 30 min and thermally curing at 80 °C for 4 h.

**Microscopic characterization.** The structures of the samples were characterized by SEM (Nova NanoSEM 430, 15 kV), Raman spectroscopy (Jobin Yvon LabRAM HR800, excited by a 632.8 nm He-Ne laser with a laser spot size of  $\sim 1 \mu\text{m}^2$ ) and TEM (Tecnai F30, 300 kV). For TEM observations, GFs were ultrasonically dispersed in ethanol for 30 min and then dropped onto a TEM grid. The edges of the graphene films tend to fold back, which allows for a cross-sectional view and consequently the determination of the number of layers of the film<sup>23–25</sup>.

**Electrical and mechanical measurements.** The four-point method is not convenient for the real-time electrical resistance testing of the samples under mechanical deformation. Therefore, the electrical conductivity of GFs and GF/PDMS composites was measured by a two-probe method. In the measurements, copper wires were embedded and connected to GFs with silver paste before infiltration with PDMS prepolymer, which enables a strong electrical contact between the copper wires and the GF and consequently a small contact resistance. The strength of PDMS and GF/PDMS films was measured with a high-precision mechanical testing system (Hounsfield H5K-S materials tester). Bend tests with different bend radii were also carried out on the Hounsfield H5K-S tester. The electromechanical stability of GF/PDMS composites as a function of bend cycles was measured by repeatedly bending the composite films with a home-made two-point bending device, where the radius of curvature was set to 2.5 mm and the bend speed was about one cycle per second. Stretch tests were carried out on the H5K-S tester at a strain rate of  $0.5 \text{ mm min}^{-1}$ . The sample size was measured using a standard caliper.

Received 2 December 2010; accepted 2 March 2011;  
published online 10 April 2011

## References

- Geim, A. K. & Novoselov, K. S. The rise of graphene. *Nature Mater.* **6**, 183–191 (2007).
- Novoselov, K. S. *et al.* Electric field effect in atomically thin carbon films. *Science* **306**, 666–669 (2004).
- Geim, A. K. Graphene: Status and prospects. *Science* **324**, 1530–1534 (2009).
- Stankovich, S. *et al.* Graphene-based composite materials. *Nature* **442**, 282–286 (2006).
- Ramanathan, T. *et al.* Functionalized graphene sheets for polymer nanocomposites. *Nature Nanotech.* **3**, 327–331 (2008).
- Ansari, S., Kellarakis, A., Estevez, L. & Giannelis, E. P. Oriented arrays of graphene in a polymer matrix by *in situ* reduction of graphite oxide nanosheets. *Small* **6**, 205–209 (2010).
- Dikin, D. A. *et al.* Preparation and characterization of graphene oxide paper. *Nature* **448**, 457–460 (2007).
- Eda, G., Fanchini, G. & Chhowalla, M. Large-area ultrathin films of reduced graphene oxide as a transparent and flexible electronic material. *Nature Nanotech.* **3**, 270–274 (2008).
- Li, X. L. *et al.* Highly conducting graphene sheets and Langmuir–Blodgett films. *Nature Nanotech.* **3**, 538–542 (2008).
- Xu, Y., Sheng, K., Li, C. & Shi, G. Self-assembled graphene hydrogel via a one-step hydrothermal process. *ACS Nano* **4**, 4324–4330 (2010).
- Lee, S. H. *et al.* Three-dimensional self-assembly of graphene oxide platelets into mechanically flexible macroporous carbon films. *Angew. Chem. Int. Ed.* **49**, 10084–10088 (2010).
- Rogers, J. A., Someya, T. & Huang, Y. G. Materials and mechanics for stretchable electronics. *Science* **327**, 1603–1607 (2010).
- Novoselov, K. S. *et al.* Two-dimensional gas of massless Dirac fermions in graphene. *Nature* **438**, 197–200 (2005).
- Zhang, Y., Tan, Y.-W., Stormer, H. L. & Kim, P. Experimental observation of the quantum Hall effect and Berry's phase in graphene. *Nature* **438**, 201–204 (2005).
- Balandin, A. A. *et al.* Superior thermal conductivity of single-layer graphene. *Nano Lett.* **8**, 902–907 (2008).
- Lee, C., Wei, X. D., Kysar, J. W. & Hone, J. Measurement of the elastic properties and intrinsic strength of monolayer graphene. *Science* **321**, 385–388 (2008).
- Berger, C. *et al.* Electronic confinement and coherence in patterned epitaxial graphene. *Science* **312**, 1191–1196 (2006).
- Sutter, P. W., Flege, J. I. & Sutter, E. A. Epitaxial graphene on ruthenium. *Nature Mater.* **7**, 406–411 (2008).
- Park, S. & Ruoff, R. S. Chemical methods for the production of graphenes. *Nature Nanotech.* **4**, 217–224 (2009).
- Hernandez, Y. *et al.* High-yield production of graphene by liquid-phase exfoliation of graphite. *Nature Nanotech.* **3**, 563–568 (2008).
- Yu, Q. K. *et al.* Graphene segregated on Ni surfaces and transferred to insulators. *Appl. Phys. Lett.* **93**, 113103 (2008).
- Chae, S. J. *et al.* Synthesis of large-area graphene layers on poly-nickel substrate by chemical vapour deposition: Wrinkle formation. *Adv. Mater.* **21**, 2328–2333 (2009).
- Reina, A. *et al.* Large area, few-layer graphene films on arbitrary substrates by chemical vapour deposition. *Nano Lett.* **9**, 30–35 (2009).
- Kim, K. S. *et al.* Large-scale pattern growth of graphene films for stretchable transparent electrodes. *Nature* **457**, 706–710 (2009).
- Li, X. S. *et al.* Large-area synthesis of high-quality and uniform graphene films on copper foils. *Science* **324**, 1312–1314 (2009).
- Bae, S. *et al.* Roll-to-roll production of 30-inch graphene films for transparent electrodes. *Nature Nanotech.* **5**, 574–578 (2010).
- Futaba, D. N. *et al.* Shape-engineerable and highly densely packed single-walled carbon nanotubes and their application as super-capacitor electrodes. *Nature Mater.* **5**, 987–994 (2006).
- Ferrari, A. C. *et al.* Raman spectrum of graphene and graphene layers. *Phys. Rev. Lett.* **97**, 187401 (2006).
- Sekitani, T. *et al.* A rubberlike stretchable active matrix using elastic conductors. *Science* **321**, 1468–1472 (2008).
- Jung, Y. J. *et al.* Aligned carbon nanotube–polymer hybrid architectures for diverse flexible electronic applications. *Nano Lett.* **6**, 413–418 (2006).

## Acknowledgements

We thank L. Ma for assisting in large-size graphene foam synthesis and discussions. This work was supported by the National Science Foundation of China (Nos 50921004, 50972147 and 50872136) and Chinese Academy of Sciences (No. KJXC2-YW-231).

## Author contributions

H-M.C. and W.R. proposed and supervised the project, W.R. and Z.C. designed the experiments, Z.C. carried out experiments, W.R., Z.C. and H-M.C. analysed data and wrote the manuscript, L.G. advised on the growth, B.L. made TEM measurements and S.P. helped with conductivity measurements. All the authors participated in discussions of the research.

## Additional information

The authors declare no competing financial interests. Supplementary information accompanies this paper on [www.nature.com/naturematerials](http://www.nature.com/naturematerials). Reprints and permissions information is available online at <http://npg.nature.com/reprintsandpermissions>. Correspondence and requests for materials should be addressed to H-M.C.